Borrower: OLS

Lending String: *SSJ,LLB,AD#,NRZ,HNE

Patron: Paul Van Delst

Journal Title: Atmospheric research

Volume: 75 **Issue:** 3
Month/Year: May 2005
Pages: 227-255

Article Author: Ulrika Willén

Article Title: Assessing model predicted vertical cloud structure and cloud overlap with radar and lidar ceilometer observations for the Baltex Bridge Campaign of CL

Borrower TN: 0

ILL Number: 118734187

Call #: Journal

Location: Online ~ Elsevier

Charge
Maxcost: 0.00

Shipping Address:
Betty Petersen Memorial Library
NOAA Center for Weather and Climate Prediction
5830 University Research Court, Room 1650, E / OC4
College Park Maryland 20740 United States

Ariel:

Email: jan.thomas@noaa.gov
Fax: 301-763-8434,

Request printed: 4/15/2014 4:40:54 PM

Billing Notes; DO NOT BILLPlease email requests to jan.thomas@noaa.gov

ELSEVIER

Atmospheric Research 75 (2005) 227–255

ATMOSPHERIC RESEARCH

www.elsevier.com/locate/atmos

Assessing model predicted vertical cloud structure and cloud overlap with radar and lidar ceilometer observations for the Baltex Bridge Campaign of CLIWA-NET

Ulrika Willén[a,*], Susanne Crewell[b], Henk Klein Baltink[c], Oliver Sievers[d]

[a]*Swedish Meteorological and Hydrological Institute, SMHI, Norrköping 601 76, Sweden*
[b]*Meteorological Institute, University of Bonn, Germany*
[c]*Royal Netherlands Meteorological Institute, KNMI, De Bilt, The Netherlands*
[d]*GKSS Research Center, Institute for Coastal Research, Geesthacht, Germany*

Received 24 April 2004; received in revised form 24 November 2004; accepted 10 December 2004

Abstract

The cloud vertical distribution and overlap of four large-scale models operating at different horizontal and vertical resolutions have been assessed using radar and lidar observations from the Baltex Bridge Campaign of CLIWA-NET. The models range from the global European Centre for Medium range Weather Forecast (ECMWF) model, to the Regional Atmospheric Climate Model (RACMO) and the Rossby Centre Atmospheric (RCA) regional climate model, to the non-hydrostatic meso-scale Lokal Model (LM). Different time averaging periods for the radar data were used to estimate the uncertainty of the point-to-space transformations of the observations. Relative to the observations, all models underestimated the height of the lowest cloud base. Clouds occurred more frequently in the models but with smaller cloud fractions below 7 km. The findings confirm previous cloud radar studies which found that models overestimate cloud fractions above 7 km. Radar-observed clouds were often thinner than the model vertical resolutions, which can have serious implications on model cloud overlap and radiation fluxes. The radar-derived cloud overlap matrix, which takes into account the overlap of all vertical layers, was found to be close to

* Corresponding author. Tel.: +46 11 4958390; fax: +46 11 4958001.
E-mail address: ulrika.willen@smhi.se (U. Willén).

0169-8095/$ - see front matter
doi:10.1016/j.atmosres.2004.12.008

maximum-random overlap. Using random overlap for vertically continuous clouds with vertical gradients in cloud fraction larger than 40–50% per kilometre gave the best fit to the data. The gradient approach could be improved by making it resolution- and cloud system-dependent. Previous cloud radar overlap studies have considered the overlap of two cloud layers as a function of maximum and random overlap. Here, it was found that the two-layer overlap could be modelled by a mixture of maximum and minimum overlap.

Keywords: Cloud vertical structure; Overlap; Cloud radar

1. Introduction

The vertical distribution of clouds has a large impact on the radiative heating and cooling rates of the atmosphere and the surface. Cloud vertical structure and cloud overlap give rise to large uncertainties when modelling climate and climate change (Weare, 2001). Due to the limited horizontal and vertical resolutions of present global and regional models, clouds need to be parameterized. New approaches have been suggested as how to deal with parameterization problems (Randall et al., 2003). Since some attempts to improve this situation incorporate high resolution (few kilometres) modelling, the ability of atmospheric models working on different horizontal scales to predict correctly cloud vertical distribution needs to be assessed. However, there is a shortage of observations of vertically resolved cloud parameters to evaluate model performance. For this reason, many recent projects have aimed to improve this situation, such as the US Atmospheric Radiation Measurement (ARM) program and the European projects CloudNET (Illingworth et al., 2004) and CLIWA-NET (Crewell et al., 2004).

In most large-scale models, clouds are assumed to be homogenous and have plane-parallel geometry, filling a grid box in a layer fully in the vertical and fractionally in the horizontal. Assumptions are needed on how the cloud fractions overlap in a grid column for calculating the cloud cover and the radiative effects of vertically stacked layers. The same rules need to be applied when comparing modelled cloudiness with satellite- and surface-based synop measurements. The various overlap assumptions can lead to large differences in the subsequent radiative heating rates of the atmosphere and the surface, and give rise to systematic errors when validating cloud cover. Barker et al. (1999, 2003) showed that there can be substantial errors of 100 W/m^2 in solar fluxes for the maximum-random overlap assumption used in many global models compared to Monte Carlo high-resolution results. However, on a global or regional scale, some of these biases cancel out and the errors on top of the atmosphere (TOA) shortwave (SW) and longwave (LW) fluxes are on the order of a few watts per square meter, even though local errors can be much larger (Räisänen and Barker, in press).

Most cloud-radiation schemes are based on maximum-random overlap as proposed by Geleyn and Hollingsworth (1979). Adjacent cloud layers have maximum overlap, and clouds which are not vertically adjacent have random overlap. For example, one would expect a convective tower contained in a grid column to be vertically stacked, while flat cumulus and cirrus are expected to be randomly placed in a grid column. Tian and Curry

(1989, hereafter TC89) showed that the maximum-random overlap assumption is supported by observations for scales up to 90 km. They used satellite observations combined with synop and aircraft measurements in their study. For larger scales, they found a tendency towards minimum overlap, as could happen for completely unrelated cloud systems.

Satellite and synop observations suffer from obscuration problems; lower level clouds can be obscured by higher clouds and vice versa. Therefore, some inherent overlap assumptions have to be made in the data processing, which might bias the results. More recently, active instruments, such as surface-based cloud profiling radars, have been used to determine vertical structure and overlap from observations (Mace et al., 1998; Hogan and Illingworth, 2000, hereafter HI00; Mace and Benson-Troth, 2002, hereafter MB02). Cloud radars have vertical resolutions which are typically smaller than those of the models and can resolve multiple cloud layers. However, drizzle or precipitation in and below the lowest cloud layer can obscure the detection of the cloud base by radar. Also, insects can lead to artificial cloud echoes. Therefore, radar measurements are combined with lidar ceilometer measurements to detect the cloud base of the lowest cloud layer. Because 35-GHz radars are in general more sensitive to insects and less affected by attenuation compared to 95-GHz radars, the use of two radars (at 35 and 95 GHz) in this study can reduce instrumental uncertainties.

The main shortcoming of ground-based radars for assessment of models is that they only measure at a single location whereas model predictions represent grid box mean values. To address this problem, the high temporal resolution observations can be converted into a spatial equivalent by assuming a mean advective wind speed—the time-averaging (or point-to-space) approach (HI00, MB02, Hogan et al., 2001). Still, it is necessary to know how representative the results are for typical model grid columns with 10–200 km horizontal scales. This can be done by varying the temporal averaging with height and time and by using complementary observations covering larger areas (e.g., satellite data for cloud tops and networks of lidar ceilometers for cloud bases). Jakob et al. (2004) suggest a probabilistic approach instead, in which the model predictions are treated as probabilistic forecasts at the observation point and the observations are left untouched. However, interpreting the results of this approach can be more complicated and the results are sensitive to the domain size and possible sampling errors. Nevertheless, it may be complementary to use both methods.

HI00 derived overlap statistics from a 94-GHz radar based at Chilbolton, UK, for a 3-month winter period. They calculated the overlap of clouds from any two layers in the "radar column." Vertically non-continuous clouds are randomly overlapped in agreement with TC89. Their results differ from TC89 for vertically continuous clouds, which were found to be in maximum overlap at close vertical separation but tending towards random overlap at 1.5–3.0 km distances, depending on the vertical and horizontal resolutions of the statistics. MB02 performed a similar analysis for longer data sets from four ARM sites equipped with 35-GHz radars. Their results support the previous findings that non-continuous clouds are randomly overlapped. However, for continuous clouds, they found no simple relation, with the overlap varying between the different geographical locations and strongly with season. Therefore, MB02 suggested that any overlap parameterization should be made in terms of cloud-system type.

In this study, we assess the cloud vertical structure of four atmospheric models using two ground-based cloud profiling radars at Cabauw for the Baltex Bridge Campaign (BBC) of CLIWA-NET during 2001. We adopt the time-average approach and use different temporal aggregation lengths of the radar data to mimic the change of mean wind speed with height. We build on the two-layer overlap studies of HI00 and MB02. Furthermore, we derive the radar "cloud overlap matrix," which contains the accumulated cloud fractions between different model levels. This matrix is used in many large-scale radiation schemes to determine the cloudy and clear parts of the column above and below a certain level, and it is used here to evaluate cloud overlap throughout the atmosphere.

2. Models

Four models from four different institutes were run for the BBC campaign period of August and September 2001: the global European Centre for Medium range Weather Forecast (ECMWF) model, the Regional Atmospheric Model (RACMO) at the Royal Netherlands Meteorological Institute (KNMI), the regional Rossby Centre Atmospheric (RCA) model at the Swedish Meteorological and Hydrological Institute (SMHI), and the non-hydrostatic Lokal Model (LM) at Deutscher Wetterdienst (DWD). The horizontal resolutions of the models vary between 7 and 50 km. Further information, such as the number of vertical levels and the typical vertical layer thickness within three height bands, is given in Table 1. The setup of the model experiments is described in more detail in Van Meijgaard and Crewell (2005).

Fractional cloudiness in all the models is the result of subgrid-scale total water variability. A prognostic scheme (Tiedkte, 1993) is used to determine the cloud fraction in the ECMWF model, whereas the other models have diagnostic schemes based on relative humidity thresholds. In the diagnostic schemes, the cloud fraction increases from 0% to 100% for completely saturated grid boxes according to some function derived from experimental data or from high-resolution cloud model results. Stratiform cloudiness is assumed to be resolved in the LM model (i.e., only 0% or 100% grid box cloud fractions can occur). Whereas ECMWF and LM are operational weather forecast models for

Table 1
The horizontal resolutions and number of vertical levels for the four models

Model	Δx (km)	Vertical levels	Layer thickness at different height intervals (m)			Time averages: $T=\Delta x/U$ (min)
			0–2.5 km	2.5–6 km	6–12 km	
ECMWF	50	60	25–340	370–550	580–780	90–**45**–30
RACMO	18	24	100–480	570–910	1060–1700	30–**15**–10
RCA	18	24	100–480	570–910	1060–1700	30–**15**–10
LM	7	35	75–350	380–550	580–920	15–**10**–5

The ranges of vertical layer thicknesses are given at three height intervals (low, mid, and high levels). The last column shows the assumed maximum, mean (bold), and minimum advective time scales, which are calculated for Δx amount of air being advected above the radar at the model mean wind speed (U) in the three height bands (10, 20, and 30 m/s).

medium- and short-term ranges, respectively, RCA and RACMO are regional climate models operating at lower vertical resolutions.

The radiative transfer for the models is calculated for clear and cloudy air separately. The radiative flux at a layer is obtained by weighting the contributions from cloudy and clear parts above and below the layer with the cloud cover. Overlap assumptions are needed to determine the cloud cover (i.e., the horizontal positions of the layer cloud fractions in the vertical column). The overlap assumptions range from maximum (minimum cloud cover) to random to minimum overlap (maximum cloud cover). Most models, like the four assessed in this study, use maximum-random overlap, whereby vertically continuous clouds are in maximum overlap and non-continuous clouds are in random overlap. Until recently, RCA was run with maximum overlap. Döscher et al. (2002) show that changing the overlap from maximum to maximum random in the atmospheric ocean-coupled version of RCA (i.e., RCA-O) led to an increase of mid-tropospheric cloud cover by 10% and increased surface downwelling LW fluxes, reducing the monthly negative bias by 4 W/m^2 and improving the sea surface temperature and ice extent over the Baltic Sea.

3. Observations and processing

We use observational data from two radars operating at different frequencies (35 and 95 GHz) that were located less than 30 m apart at Cabauw during the BBC campaign. The 35-GHz KNMI radar was operated continuously, but due to failure of the power amplifier, it was not available for 2 weeks in August. The 95-GHz GKSS radar (Quante et al., 2000) was operated only during daytime, but not in clear-sky conditions or in precipitation. The reflectivity data from the KNMI radar are available every 10–20 s at a vertical range gate spacing of 90 m, with the lowest range gate at 217 m. The 35-GHz profiles used in this study are a combination of data from two modes: one uncoded mode and one mode with pulse coding applied. The maximum range for the uncoded mode was around 11 km, whereas the coded mode reaches only up to 5.8 km. As the coded mode is more sensitive than the uncoded mode, the combined profile has a break in sensitivity at 5.8 km. For the GKSS radar, the integration time is 5 s with a vertical range gate spacing of either 37.5 m or 82.5 m. The lowest gate is at 494 m. The sensitivity of the radars is described by the minimum detectable reflectivity, which increases with the distance (height) squared. At 5 km of altitude, it is −45 dBZ for the GKSS radar and −40 dBZ and −47 dBZ for the KNMI uncoded and coded modes, respectively.

Most results we present are derived from the KNMI radar since continuous time series are available. To analyze some results in more detail, the GKSS radar data are useful for certain time intervals when it operated at higher vertical resolution. A binary cloud mask in the time-range domain is generated from the radar data by applying a cloud masking algorithm. Since the radars cannot identify the cloud base in the case of precipitation or even light drizzle, a collocated Vaisala CT75K lidar ceilometer was used to identify the lowest cloud base for drizzle events. Any radar signal below the lidar cloud base was removed. This also helps to reduce, but not eliminate, contamination of the radar signal due to insects (Hogan et al., 2001). The sensitivity of the radars is strongly reduced (10–15

dBZ) when precipitation falls on the shroud of the radar antenna. This can affect the detection of the upper part of clouds in these conditions. Therefore, similarly to HI00, the radar data were not used for rain rates (measured by a rain gauge) larger than 0.5 mm/h.

For evaluating model vertical cloud distributions, we create radar grid box mean values by averaging the radar observations over different time intervals to mimic the different horizontal resolutions of the models. We also average over different numbers of range gates to account for model vertical levels (same technique as Hogan et al., 2001). The ratio of the number of cloud-filled pixels (or range gates) to the total number of pixels in each "grid box" gives a volume fraction which corresponds to the model cloud fraction. Because the wind speed varies with time and height, in principal, the time for the temporal average should vary accordingly to produce horizontally equal sized amounts of air at all levels. For simplicity, we choose to calculate the radar cloud fractions for three fixed time scales for each model, depending on the mean observed wind speed in the three height intervals listed in Table 1.

4. Cloud vertical distribution

First, we show the mean vertical cloud fractions for each model grid column closest to Cabauw for the August and September 2001 periods (Fig. 1). The model cloud fractions can be interpreted as the percent of time the model sky was covered with clouds at different layers and they can be compared with the occurrence of hydrometeors in each 90-m vertical range bin from the KNMI radar (also shown in Fig. 1). The models capture some of the vertical structure, especially the difference between the two periods. August was a fairly sunny month with convective activity at Cabauw, while September was more overcast with persistent low level cloudiness, fog and far more precipitation than usual. All models overestimate the occurrence of high clouds (above 7 km) and underestimate clouds at mid-levels (mainly for September), similar to what Beesely et al. (2001) and Hogan et al. (2001) found for the ECMWF model for the Arctic and England, respectively. Between 400 m and 2 km all models overestimate cloud occurrence. Below 400 m, all models tend to underestimate cloud fraction (also similar to Hogan et al., 2001).

In order to study the forecast skill of the models, we calculated the mean error (bias) and the root mean square error (RMSE) for the models compared to the radar-derived time series of cloud fraction (Fig. 1). For this purpose, the radar volume cloud fractions were calculated for each model vertical layer assuming the mean mid-tropospheric advective time scale (Table 1). The bias structure is fairly similar for all models, although RCA has slightly less overestimation at high levels. The underestimation of clouds at mid-levels in September occurs at slightly higher altitudes (3–6 km) for the ECMWF model than for the regional models (2–6 km) and for LM (2–7 km). In addition, RCA and LM had narrower lower-level maxima than the radar in September.

The random errors are larger than the mean values of cloud fraction, but as Hogan et al. (2001) point out, it might be too rigorous to expect the models to perform accurately to within 10–60 min and at one specific model level. Hogan et al. (2001) modified the model cloud fractions to account for some of the known limitations of the radar measurements. For example, high thin clouds may be undetected by the radar and can potentially be

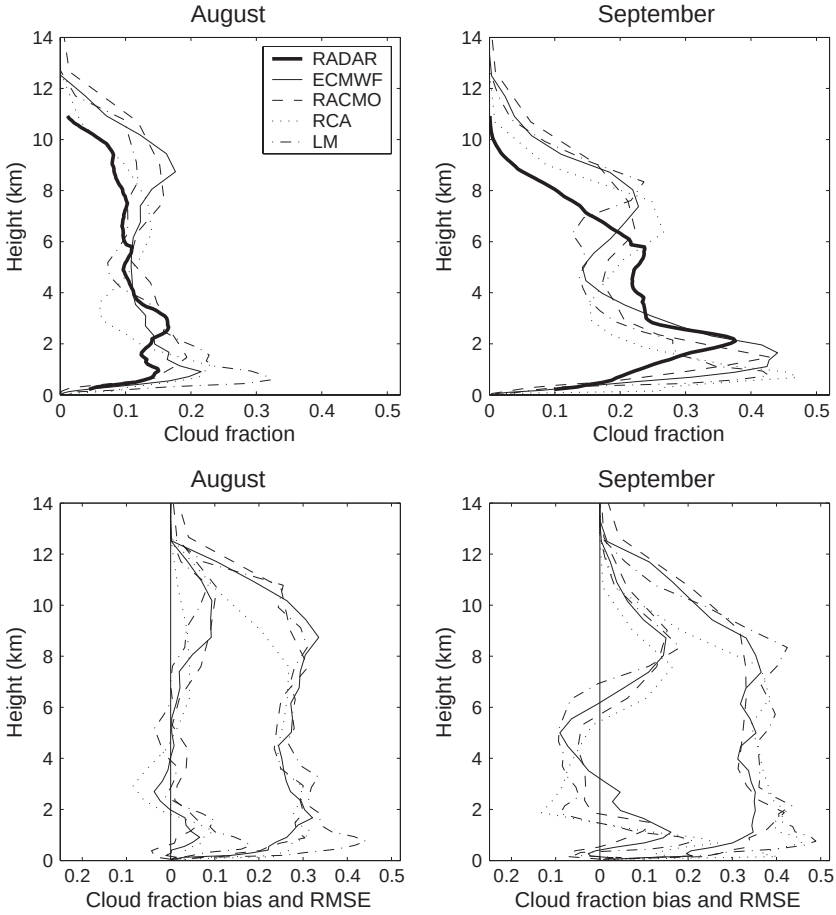

Fig. 1. Mean cloud fractions (top row) for the original 90 m resolution data of the KNMI radar for August and September. The model values are given at their specific layer resolution. The bias and RMSE between the time series of model predicted and observed cloud fractions (bottom row) are derived for each model mean advective time scale (see Table 1).

excluded from the model and observation comparison. The model underestimation of clouds at mid-levels could be due to precipitating ice crystals or snowflakes, which are included in the radar-derived cloud fractions but not in the model fractions. Here, we have left the model outputs unchanged. However, we do investigate the validity of the time-averaging approach, as will be presented next.

Even if the model vertical distributions of mean cloud fractions were correctly predicted, the assumption of fixed advection velocities can cause discrepancies between models and observations. The averaging period for the radar should be adjusted for the observed wind speed increase with height as the sampling volume becomes larger at higher wind speeds. Therefore, we used the maximum and minimum time averages (corresponding to the minimum and maximum wind speeds in the grid column) from

Table 1 to obtain a range of probable realizations from the observations. In order to determine if the mean errors were due to differences in cloud occurrence or cloud amount, we calculated the "cloud frequency of occurrence" and the "cloud amount when present" (Fig. 2), similar to Hogan et al. (2001) for the different time averages. As illustrated in Fig. 2, the cloud occurrence and cloud amount for the observations are fairly insensitive to the length of the time intervals. The longer time averages contained fewer clear-sky cases and therefore they have smaller cloud amounts and slightly higher frequencies of occurrence than the shorter time averages.

The model frequency of occurrence should be compared to the observed upper limit (longer time averages) at low levels and observed lower limit (shorter time averages) at high levels to take into account the change of wind speed with height. On the other hand, since the observed cloud amount decreased for longer time averages, the model amount should be compared to the lower limit (longer time averages) at low levels and upper limit (shorter time averages) at high levels. The models are similar to each other and do not fall into the range of the observations, although the model errors are smaller if we compare them with the different time averages for the radar at different heights than if we would have used one single time average. The models overestimate the occurrence of clouds at low and high levels and underestimate the amount of cloud between 1 km and 6 km. The errors above 7 km appear to be due to both too high occurrences and too high amounts when present. At higher altitudes, cloud amount was smaller for RCA and closer to the observations. Note that we cannot rule out the possibility that the plentiful precipitation in September might have affected the detection of clouds at higher levels. The amount of rain in September was three times its 30-year mean climatological value. However, almost half of it was collected on a single day, September 19. Most data from this day were removed from the analysis due to the high rain rates.

To further investigate the deviations between radar and model cloud fractions, we compare the frequency distributions of cloud fractions within the three height intervals of Table 1 (Fig. 3). Again, the maximum and minimum time averages of the observations for each model are employed. Ideally, the model distributions should fall within this "uncertainty range" of the time-average approach. Generally, the model distributions are more skewed than the observations and the occurrence of smaller cloud fractions (<50–60%) is overestimated at all heights by all models. This is contrary to Hogan et al. (2001), who only found a slight skew for the ECMWF model compared to the radar observations. They added a snow contribution to the model cloudiness, which increased the cloud amounts at mid-levels and removed high thin model clouds, thereby potentially improving the comparison.

The models underestimate clear-sky conditions and the occurrence of overcast especially at mid-levels, which also is found by Van Meijgaard and Crewell (2005) with a different set of instruments. Fractional cloud covers in RACMO that exceed 80% require that the grid box mean relative humidity be within 1% of saturation. These conditions are hardly met in the model, which explains the "cut-off" at this value in the figure. The RCA model has a smaller overestimate of overcast skies at high levels, explaining the previously noted results in Fig. 2. The good agreement for the LM in Fig. 3l is due to an underestimate of cloud amount between 6 and 8 km and overestimate above 8 km (cf. Fig. 2l). As pointed out in earlier observational studies (e.g., TC89), the probability of either

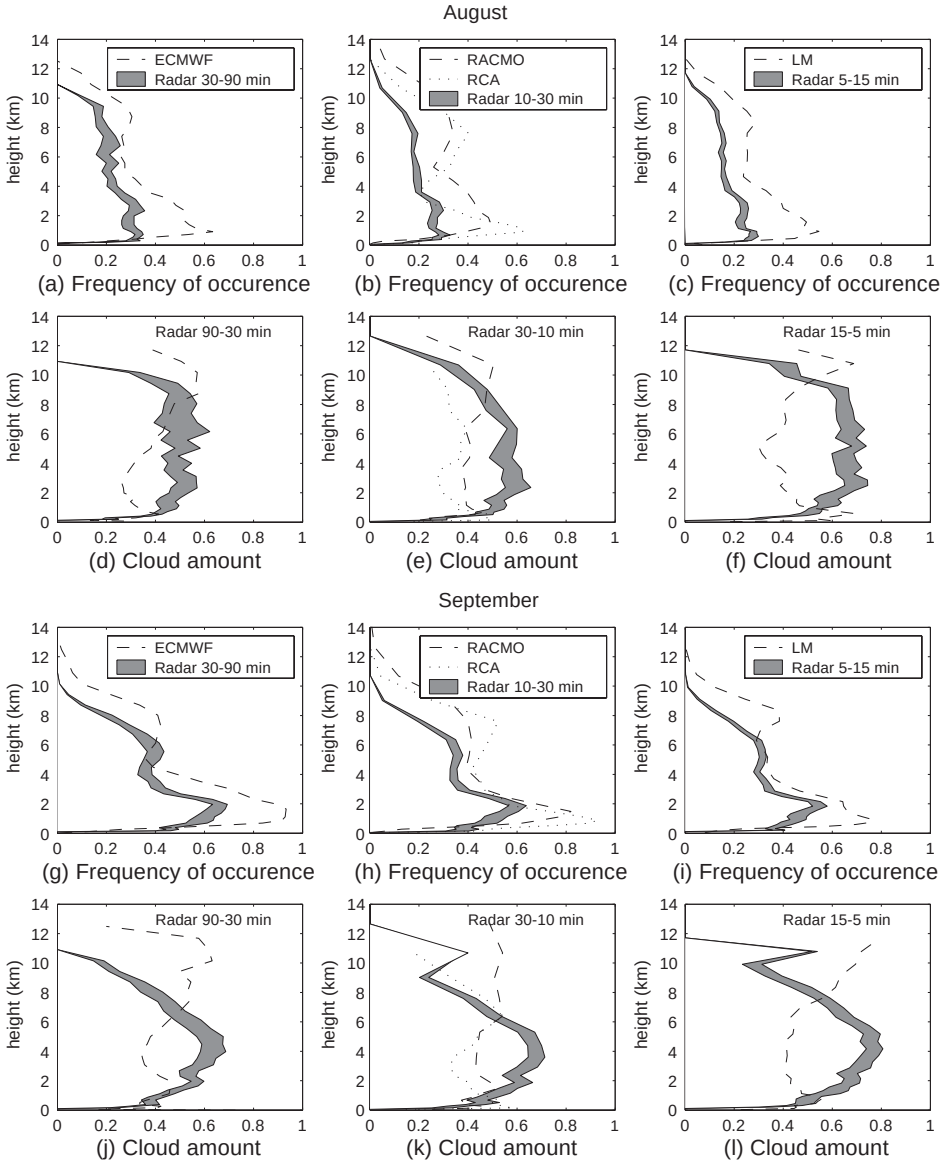

Fig. 2. Frequency of cloud occurrence and amount when present (>5%) for ECMWF (left), LM (right), RCA and RACMO (middle), and the KNMI radar at the corresponding model vertical resolution. The grey shaded areas indicate the possible variations in the observations due to changes in advection speed with height. For the cloud occurrence, the lower limit of the bands corresponds to the shorter time averages and the higher limit to the longer time averages, respectively. The opposite order of the time averages is valid for the observed cloud amount as indicated in the legends.

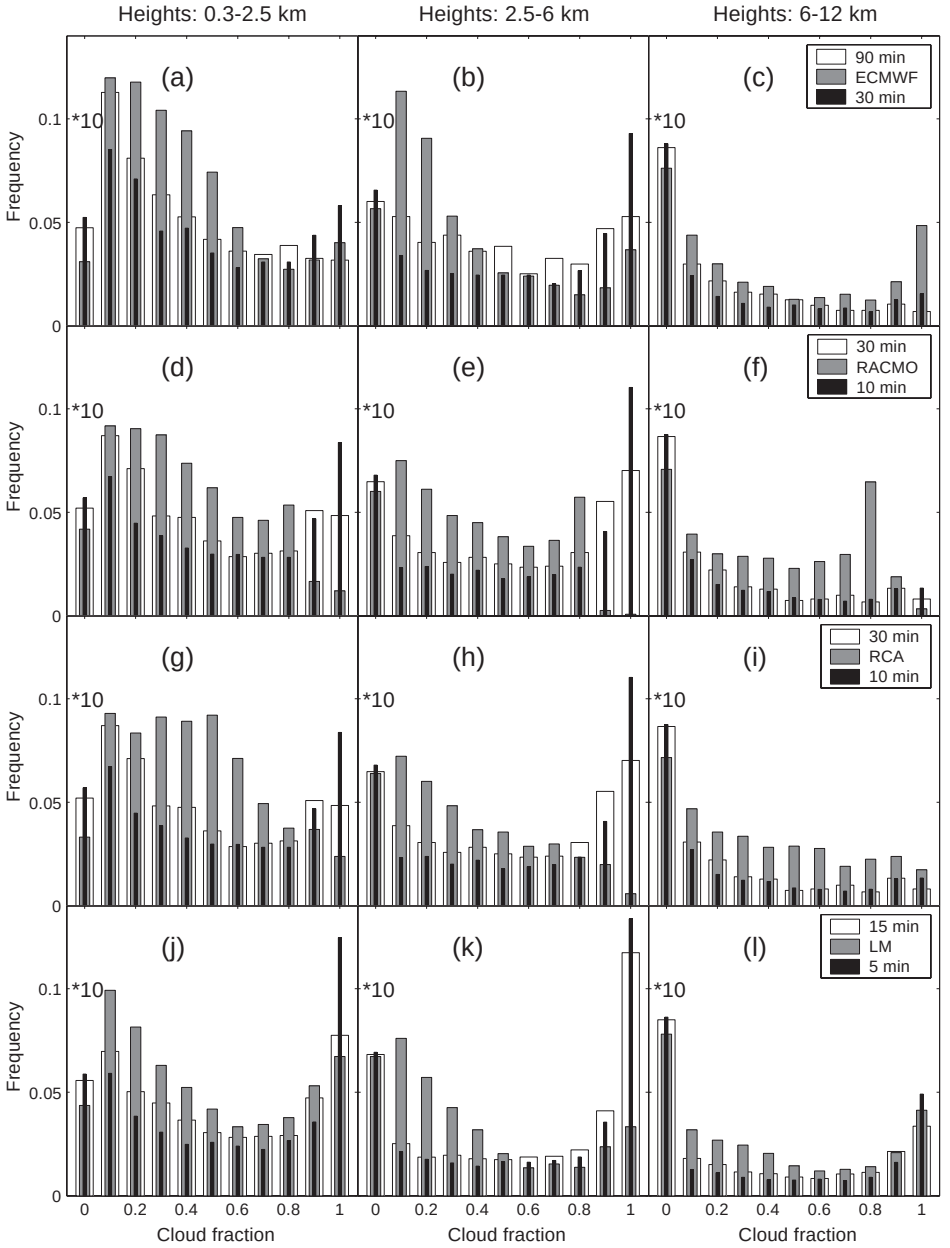

Fig. 3. Probability of occurrence distributions of the cloud fractions for ECMWF, RACMO, RCA, and LM (top to bottom row), together with the corresponding radar observations, for low, mid, and high clouds for September 2001. The model distributions (grey bars) are compared to the observations averaged according to their minimum (black bars) and maximum (white bars) advective time scales. The first group of bars (i.e., clear sky) should be multiplied by 10.

clear-sky or overcast decreases as the area increases. This can be seen here by comparing the two most extreme radar time averages (i.e., 5 min (black bars in the bottom panel) and 90 min (white bars in the top panel)). These time averages correspond to length scales of 5 km and 92 km for the mean observed wind speed of U~17 m/s at mid-levels. The frequency distributions are similar for the August period (not shown).

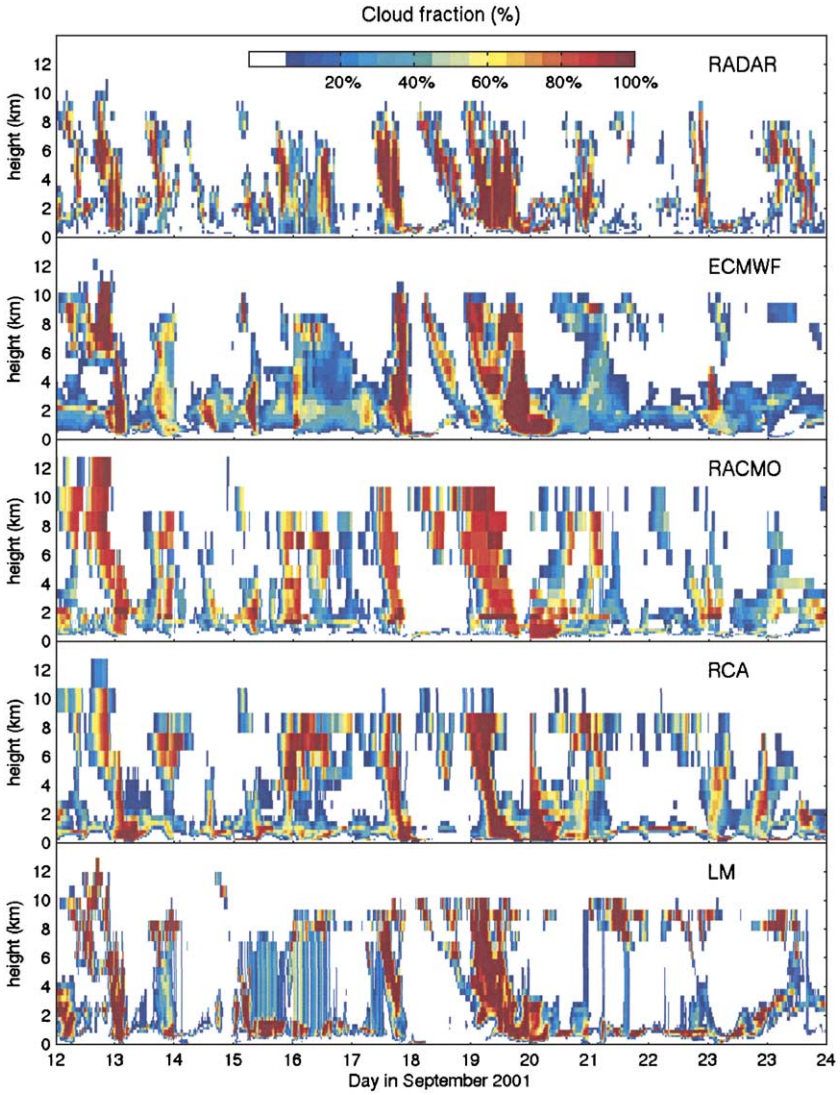

Fig. 4. Time series of vertical cloud structure for the KNMI radar and for the models for 10 days in September 2001. The radar cloud fractions are plotted for 60 vertical levels and 60-min temporal averages, corresponding to the resolution of the ECMWF model.

All the identified errors in model cloud fraction compared to the radar-derived cloud fractions can be illustrated in a 13-day time series for September (Fig. 4). Even though there is a strong correlation between the observed and model cloud fractions, overestimation of high clouds by the models is clearly visible. High thin clouds may be undetected by the radar due to a combination of their small ice particle size and the reduced radar sensitivity with height. As mentioned previously, Hogan et al. (2001) excluded from their comparisons ECMWF model clouds with ice water content less than the particle-size dependent minimum value detectable by the radar. This improved the agreement at high levels, but still there was an overestimate of up to a factor of 2. The KNMI 35-GHz radar has better sensitivity than the 94-GHz radar used by Hogan et al. (2001), but we also find an overestimate of model cloud-top height of 1.5 km for both August and September when high thin clouds are excluded (not shown).

All models capture the structure of the observations, but they overestimate the occurrence of small cloud fractions at mid-levels. The results illustrated in Fig. 3 are dependent on the chosen height intervals, as clearly visible for the LM model in Fig. 4. Following Hogan et al. (2001), we added a snow fraction to the ECMWF model output when the "critical snow flux" exceeded 0.05 mm/h. The cloud amounts at mid-levels increased, leading to excessive cloud fractions due to the overestimate of cloud occurrence below 4 km (Fig. 2g). Overall the agreement with the radar observations was not improved for the BBC time period. The coarse vertical resolutions of the regional models might partly explain the low frequency of overcast conditions noted at mid-levels (e.g., Fig. 3).

The overestimation of cloud occurrence at low levels, especially by the RCA and LM models for September, could be due to an underestimation of the planetary boundary height in the models as noted by Van Meijgaard et al. (2001). The current turbulence scheme in RCA only includes dry variables and might not be active enough. Re-running the RCA simulation with increased vertical resolution (40 and 60 levels) raised the cloud base height (not shown). The thick, somewhat diluted, low level clouds of the ECMWF model (Fig. 4, also visible in the occurrence plots in Fig. 2g) could be a result of too much mixing in the boundary layer. All models underestimated the height of the lowest cloud base. This was also verified from measurements of cloud bases by six lidars in a network surrounding Cabauw covering a 100 km×100 km area. As the lidars indicate (not shown), the cloud fields were fairly homogeneous across the area, which supports the point-to-space transformation used to obtain the radar cloud fractions.

5. Volume and area cloud fractions

In Section 4, we compared the model cloud fractions with the radar-derived volume fractions. For the overlap statistics of the whole grid column we first need to know the horizontal extent of the observed clouds at different altitudes, the cloud cover, or "the area fraction." Model clouds are assumed to fill the vertical extent of each model layer; therefore, the volume (V) and area (A) fractions are equal (as sketched in Fig. 5a). The observed volume and area fractions will differ if the observed clouds are sheared or thinner than the model vertical resolutions as illustrated in Fig. 5b–i. The cloud layer thickness

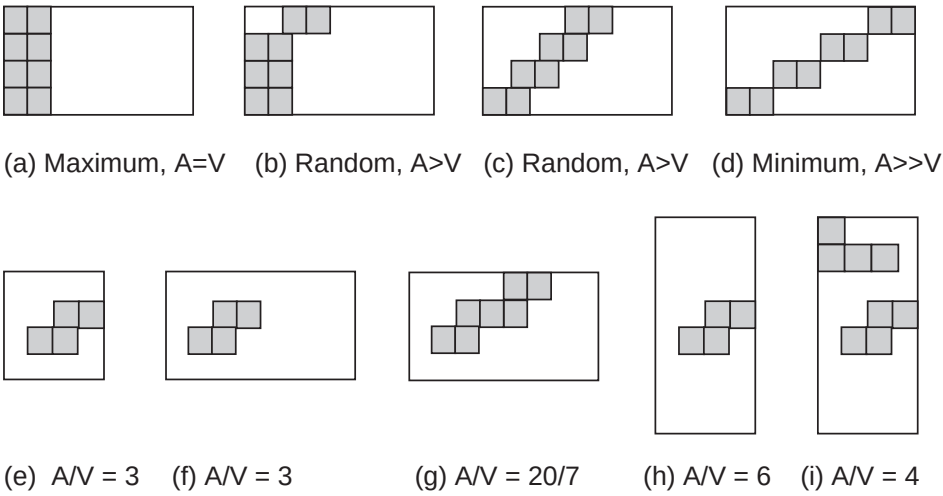

Fig. 5. Schematic figure of a cloud (grey pixels) in a grid box where each pixel corresponds to the radar vertical resolution (90 m) and, in the horizontal, the radar–lidar temporal resolution (30 s) in: (a) sub-grid scale maximum overlap (i.e., a plane-parallel cloud); (b and c) subgrid-scale random overlap; and (d) subgrid-scale minimum overlap. Changes to the A/V ratio occur for decreased temporal resolution; compare (e) with (f) and (g) and, for decreased vertical resolution, compare (e) with (h) or (i).

frequency distributions for both radars show similar results for the BBC period (Fig. 6), even though the GKSS radar was mainly operated at daytime. About 60% of the cloud layers had thicknesses less than 1 km and 25–35% were thinner or equal to three radar range gates (i.e., 270 m). Other studies using cloud radars show similar thickness distributions and mean thicknesses for different cloud types—1.6 km for cirrus (Mace et al., 1997); 0.8–1.0 km for stratus (Dong et al., 2000); here 1.2–1.4 km for all clouds. Since the observed clouds were thinner than the typical model vertical resolutions, they will deviate from the plane-parallel (PP) assumption (i.e., they do not fill the grid box in the vertical). Here, we only consider the geometrical extent of the PP assumption and not the subgrid variability of the total water content.

To investigate if the geometrical deviation from the PP assumption could affect the overlap, we calculated the radar volume and area fractions (Fig. 7) for different vertical (as well as temporal) resolutions that correspond to typical model vertical resolutions at low, mid, and high levels (Table 1). The radar area fractions are determined from the horizontal projection of cloud elements in each grid box (HI00, MB02). For coarser vertical resolution, there is a larger difference between the volume and area fractions (Fig. 7, left column). This is further illustrated by the scatter in the direct comparison of volume and area ratios (Fig. 7, middle and right columns). For true plane-parallel clouds, which fill the box in the vertical, the ratio would be one (cf. Fig. 5a). The other extreme scenario would be clouds that fill the grid box in the horizontal while only being one range gate thick in vertical extent (e.g., as in Fig. 5d). These two extremes, marked by the two limiting straight lines in the scatter plots in Fig. 7, correspond to subgrid-scale maximum and minimum overlap, respectively. Calculating subgrid-scale random overlap for the cloud volume in Fig. 5a with the cloud pixels at all vertical range gates displaced (Fig. 5c) and

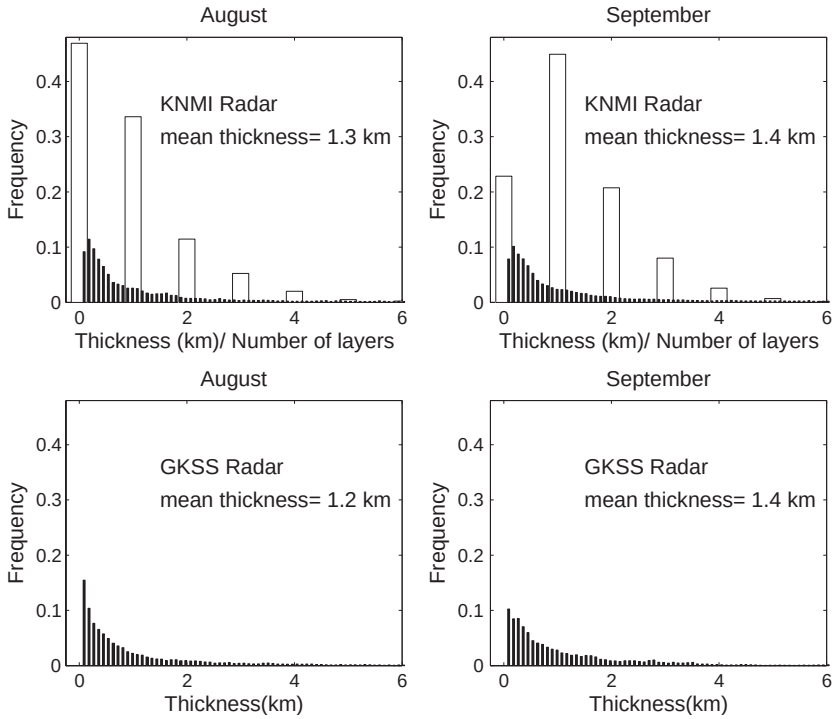

Fig. 6. Frequency distributions of cloud thickness (black bars) for the raw resolution data derived from the KNMI (top) and GKSS (bottom) radars for August (left) and September (right). The frequency distribution for the number of cloud layers (white bars) is also given for the continuously operating KNMI radar.

for the cloud pixels at only one vertical range gate displaced (Fig. 5b) gave a larger and smaller limit for random overlap as shown by the curved full lines in the scatter plots.

The observed values are close to maximum overlap for the vertically thin grid boxes (Δz=270 m), as expected from the cloud layer thickness statistics. If we consider a cloud, such as in Fig. 5e, reducing the temporal resolution would give the same A/V ratio if no other cloud filled pixels were included (Fig. 5f). However, if other cloud elements are incorporated into the averages (Fig. 5g), the volume fraction could decrease slower than the area fraction, thereby making the ratio smaller and the clouds more plane-parallel as noted in the scatter plots (Fig. 7, right column). For lower model vertical resolution with a grid box containing more radar range gates, higher ratios between area and volume fraction can occur. If we again consider the isolated cloud in Fig. 5e, decreasing the vertical resolution (Fig. 5h) would result in a decrease of volume fraction whereas the area fraction would remain the same, leading to a ratio that approaches the minimum overlap line. Incorporating other cloud elements can also give a larger A/V ratio (Fig. 5i). In Fig. 7, the observed values are close to random or even minimum overlap for the thick grid boxes (Δz=540 m and 1440 m).

The minimum and random overlap sketches in Fig. 5b–d are drawn for comparison with Fig. 5a and are not necessarily realistic scenarios (e.g., the large area to volume ratios

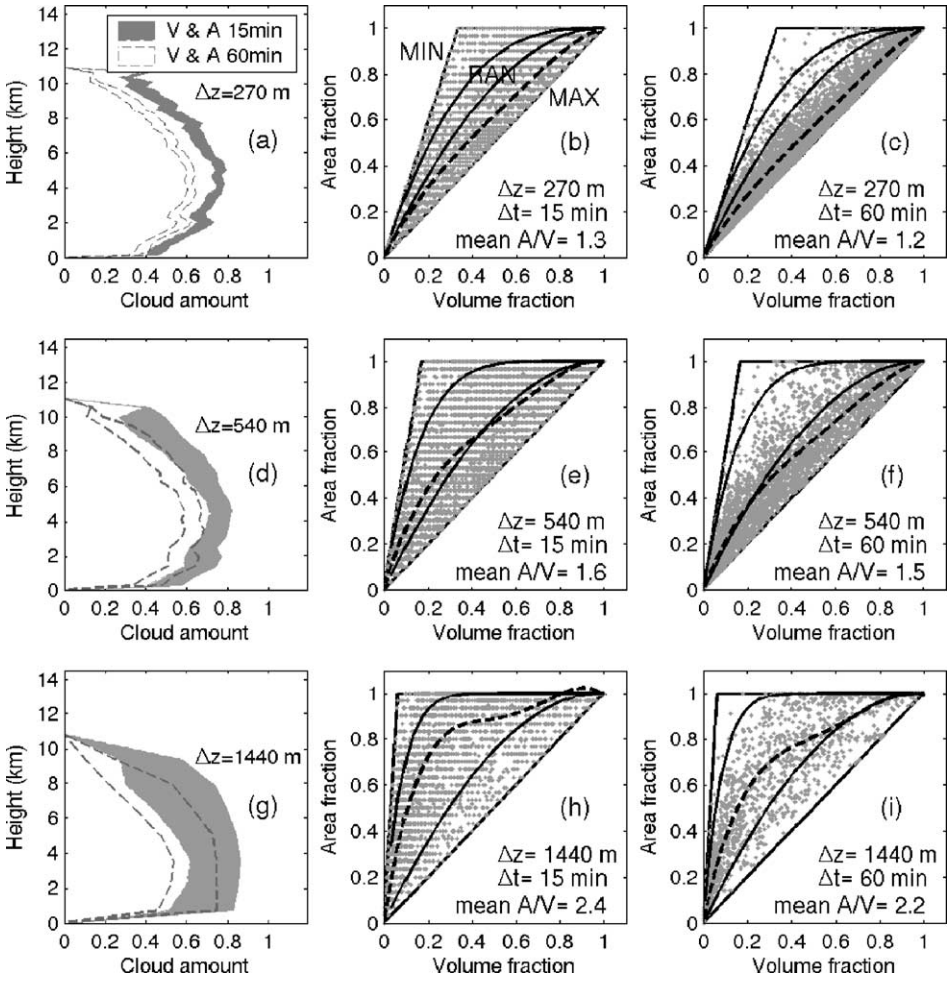

Fig. 7. Cloud amount for September (left column) as a function of height derived from radar observations for grid boxes with 270 m, 540 m, and 1440 m vertical resolutions for 15 and 60 min time averages. The lower limit of each band corresponds to the volume mean fraction and the higher limit to the area mean fraction. Scatter plots of the area (ordinate) to volume (abscissa) fractions for all grid boxes are presented for the two different time averages of 15 min (middle column) and 60 min (right column). The black dashed lines in the scatter plots are polynomial fits to the data for guidance. The $A=V$ line illustrates subgrid-scale maximum (MAX) overlap (i.e., plane-parallel clouds of the type in Fig. 5a). The steepest line indicates subgrid-scale minimum (MIN) overlap, $A=KV$ (Fig. 5d), where K is the number of radar range gates in the "grid boxes" (i.e., 3, 6, and 16 for 270 m, 540 m, and 1440 m resolutions, respectively). The curved full lines show the upper limit, $A=(1-(1-V)^K)$(Fig. 5b), and lower limit, $A=(1-(1-V)^2)$, of subgrid-scale random (RAN) overlap. The original temporal resolution of the lidar–radar data (30 s) produces stepwise ratio changes visible for the 15 min averages since the area fraction can only change by 1/30.

in Fig. 7) (points close to the minimum overlap line, middle and right column) are more likely due to a single cloud layer with cloud filled pixels at the same height. The frequency distributions show that about 10% of the clouds were only one range gate thick (Fig. 6)

and there was only one cloud layer 34% and 45% of the time for August and September, respectively (Fig. 6, top row).

These results have implications for model overlap calculations. Even if a model predicts the correct volume amounts, treating the clouds as plane-parallel in the model would lead to an underestimation of cloud cover and overestimation of the overlap, especially for the RACMO and RCA with only 24 vertical levels and grid boxes of up to 1.7 km in vertical extent. In Section 6, we will mainly consider the observed overlap, since all the models in this study assume that clouds are vertically resolved and do not consider any subgrid-scale positioning of the model cloud fractions.

6. Two-layer cloud overlap

Most radiation schemes assume maximum overlap for vertically continuous layers and random overlap for clouds separated by clear layers. Both these assumptions can give errors in cloud cover and thereby in the radiation fluxes. For non-continuous clouds, the overlap might be overestimated (cloud cover underestimated) for large grid boxes, since it is more likely that unrelated clouds are included and the overlap could be minimum. For continuous clouds, the overlap might also be overestimated. Many observed clouds are vertically sheared and have a characteristic "slanted" appearance in the radar time series. If such a cloud is contained inside a "grid box," considering vertical layers farther and farther apart, the overlap becomes more random and using maximum overlap would underestimate the cloud cover.

In order to quantify this last effect, HI00 considered the overlap of every possible pair in the radar vertical grid columns. They used grid box area fractions to calculate the mean combined cloud cover of any two grid layers assuming minimum, random, and maximum overlap, and compared the results with the observed overlap, C_{obs}, from the raw radar data. The data were sorted according to the vertical separation of the levels and separated into vertically continuous clouds and non-continuous clouds. They expressed the overlap in terms of a maximum-random (MR) overlap parameter, α, as:

$$C_{\mathrm{obs}} = \alpha * C_{\mathrm{max}} + (1 - \alpha) * C_{\mathrm{ran}}. \quad (1)$$

Here, we consider the overlap of pairs of vertical boxes following HI00 and MB02. Negative values of the overlap parameter can occur for clouds in minimum overlap, which have a larger combined cloud cover than clouds in random overlap. To avoid this, the observed overlap can also be expressed as a mixture of maximum and minimum overlap. We defined the maximum–minimum (Max–Min) overlap parameter, β, in the same way as for α but with the random overlap cloud cover, C_{ran}, replaced by the minimum overlap cloud cover, C_{min}:

$$C_{\mathrm{obs}} = \beta * C_{\mathrm{max}} + (1 - \beta) * C_{\mathrm{min}}. \quad (2)$$

The overlap parameters were calculated as a function of vertical separation for the BBC period using vertical grid boxes with thicknesses between 180 and 1440 m and for temporal averages of 5–120 min (corresponding to horizontal spatial averages of 5–122

km). The results are shown in Fig. 8 for two vertical and temporal resolutions for September 2001.

For non-continuous clouds (Fig. 8a and d), α was almost zero, indicating that the clouds were close to random overlap in accordance with HI00 and MB02. For vertically continuous clouds (Fig. 8b and e) the overlap varied from maximum at small separations towards random at larger separations, also very similar to HI00. HI00 identified an e-folding or "de-correlation" distance, Δz_0, by fitting an exponential function to the data:

$$\alpha = \exp(-\Delta z/\Delta z_0), \tag{3}$$

where Δz is the vertical separation between two layers. In HI00, Δz_0 ranged from 1.5 km to 3.0 km depending on the size of the grid boxes. Their suggested exponential fitted curves are also shown in Fig. 8b and e, where it can be seen that our data exhibit similar de-correlation lengths. Cabauw is geographically close to Chilbolton, which perhaps explains the good agreement especially for vertical separations less than 6 km. The alternative maximum–minimum overlap parameter was fairly constant at 0.5 for non-continuous clouds. For continuous clouds, β was also close to 0.5 with a tendency to maximum overlap at smaller separations. The overlap changes from maximum to halfway in between maximum and minimum at "de-correlation lengths" similar to what was observed for α.

Decreasing the temporal resolution, HI00 obtained larger de-correlation distances (i.e., more maximum overlap), which always would occur for an isolated cloud contained in a grid box, as illustrated in Fig. 5e and f, if we assume that the sketch represents a grid column cross section with four model vertical levels. However, as MB02 points out, if other non-related cloud elements are incorporated into the same average, the overlap could be smaller, approaching random or even minimum overlap (cf. Fig. 5e and g). For the resolutions plotted in Fig. 8b and e (with horizontal grid sizes increasing from about 20 km to 122 km), there are tendencies towards minimum overlap ($\alpha<0$) in the range of separations from 5 to 8 km. Beyond 8 km of vertical separation, α is positive, indicating a combination of maximum and random overlap. The variation of α for $\Delta z>6$ km might not be statistically significant. However, considering the average cloud thickness distributions for the radar grid boxes (Fig. 8c and f), about 20–25% of the clouds were thicker than 6 km for the 122 km grid sizes.

The raw data (Fig. 8c and f) have a clear exponential decay and reducing the temporal or vertical spatial resolutions increased the frequency of thicker clouds. The cloud thickness distributions changed with averaging and became more bimodal with a maximum at 2.5 km and a smaller secondary maximum around 7 km. As previously mentioned, this could be due to the grid boxes either containing thick, but inhomogeneous, cloud, or having unrelated cloud elements averaged within it. Investigating daily and hourly time series of the radar reflectivity for the BBC period showed that there were some occasions of thick clouds up to 7–8 km. However, due to false cloud free areas, which could occur higher up if the radar signal is damped by rain at lower levels, or natural small scale variability, the clouds do not appear as thick for the raw data as they do for the spatially and temporally averaged data. These thick clouds were in maximum overlap even

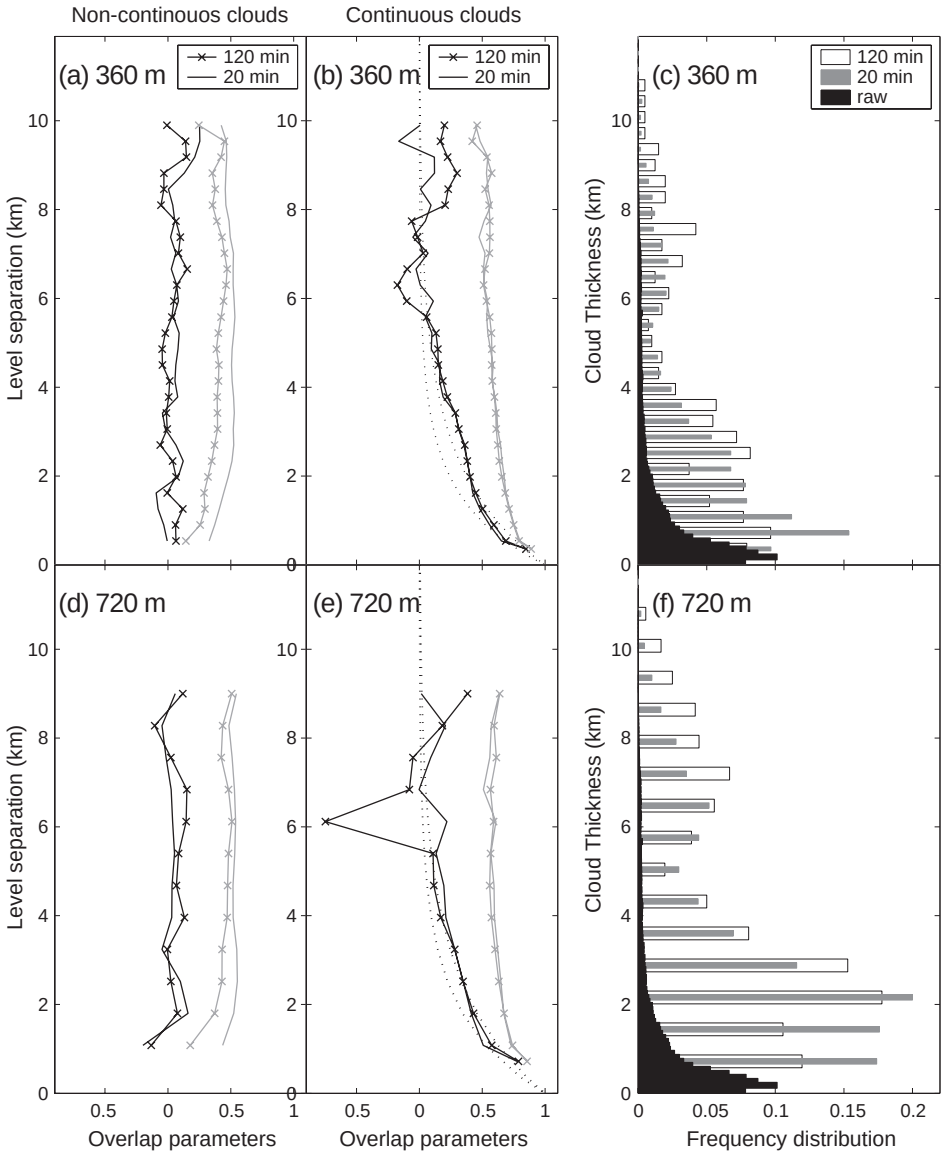

Fig. 8. The overlap parameters for vertically non-continuous (left) and continuous (middle) clouds for 360 m (top) and 720 m (bottom) vertical resolution grid boxes for two different time resolutions of 20 min and 120 min for September. The maximum-random parameters, α, are given in black and the maximum–minimum parameters, β, in grey. The dotted lines show the exponential fit to the maximum-random parameter as suggested by HI00, with the de-correlation distances (Table 1 HI00) of 1.40 km and 2.04 km for 360 m, and 1.68 km and 2.90 km for 720 m for 20 min and 120 min, respectively. The corresponding cloud thickness frequency of occurrence distributions for the averaged data is shown together with the "raw" distributions (same as in Fig. 6) in the right column.

at large vertical separations, explaining the tendency towards maximum overlap at separations above 8 km in Fig. 8b and e. The two-layer overlap statistics were only calculated between cloud layers with less than 100% cloud area fractions (all overlap assumptions are the same for clouds of 100% area fractions). Therefore any thick cloud with 100% cloud fraction in the interior will only contribute to the overlap statistics when we approach the cloud top and bottom.

β is fairly constant with separation distance compared to α. Therefore, fitting a curve to the β-parameter data could yield an overlap parameter which is less sensitive to changes in temporal and vertical resolutions. Even if random overlap might appear as a better physical choice, for larger scales, some clouds could be in minimum overlap. TC89 suggested a linear mixing of 50% random and 50% minimum overlap if the cloud cover is larger than 70% for grid sizes exceeding 45 km, since these grid boxes contained many single cloud layers but at different heights (i.e., the clouds were in minimum overlap).

The de-correlation distance for continuous clouds can also be identified in the mean subgrid-scale overlap statistics in Fig. 7. The mean subgrid-scale overlap varied from close to maximum overlap for thin grid boxes towards random overlap for thicker grid boxes, or, as in this section, as Δz becomes larger. This could be due to continuous clouds having less correlation at larger layer separations as suggested by HI00, or that several thin single layers are being incorporated into the averages as the grid boxes becomes thicker (i.e., the clouds are not truly vertically continuous as in Fig. 5i). The subgrid-scale overlap (i.e., the area fractions in Section 5) could be expressed as a function of the volume fractions using some combination of the different overlap assumptions plotted in Fig. 7 similar to what was made for the two-layer cloud cover (Eqs. (1) and (2)).

The overlap parameters can be viewed as indirect measures of the cloud thickness frequency of occurrence distribution, and the de-correlation length for a unimodal distribution is a measure of the most common cloud thicknesses. September was dominated by frontal and boundary layer clouds of 2–3 km thicknesses and the de-correlation lengths of 1.5–3.0 km were of similar order. Since the distribution of "continuous" clouds changes as the resolution changes, it might not be appropriate to use one de-correlation length derived from two-layer statistics for modelling the overlap, especially for cloud distributions with more than one dominating cloud thickness. We turn to this issue in Section 7 where we investigate the overlap of all vertical levels in a grid column.

7. Cloud overlap matrix

Even if the two-layer overlap statistics might be determined with confidence for different geographical locations, when all model cloud layers are considered, two-layer statistics are not sufficient to characterize a cloud field. As a result, many large-scale model radiation schemes utilize a cloud overlap matrix. The matrix contains the accumulated cloud cover between any two levels in the atmosphere; therefore, the amount of clear and cloudy sky above and below any layer can be determined for shortwave and longwave calculations (Manabe and Strickler, 1964). We use the cloud

overlap matrix to evaluate existing overlap assumptions and to test new combinations of overlap.

First, we consider the most commonly used parts of the cloud matrix—the cloud cover viewed from the surface and from the TOA, which are used when comparing the model cloud cover with satellite and synop observations. This cloud cover is shown in Fig. 9a and b for different overlap assumptions, ranging from maximum (MAX, Eq. (4)),

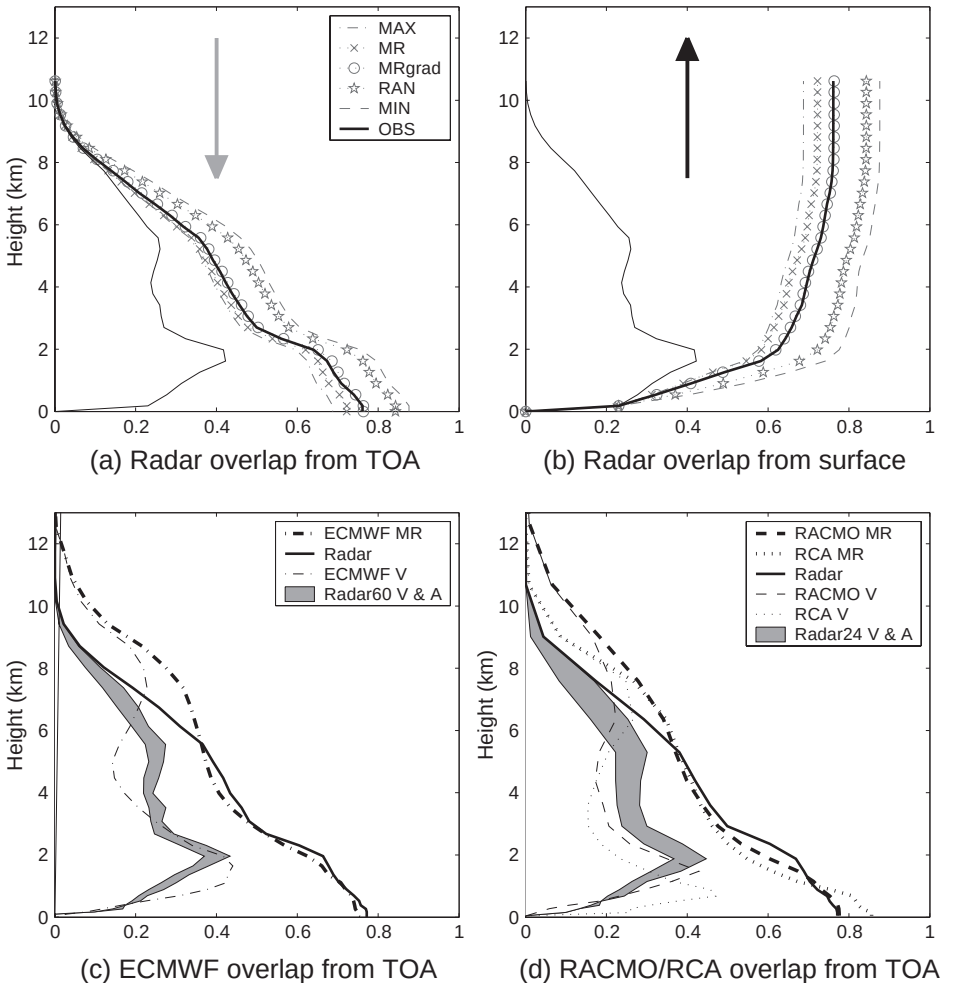

Fig. 9. Accumulated cloud area fractions or overlap from (a) TOA and (b) the surface derived from the KNMI radar for September (black thick solid line). The cloud cover calculated from the different overlap assumptions using the radar area fractions is represented by the grey lines. The radar mean area cloud fraction for each layer is shown for reference (black thin solid line). Model maximum-random overlaps for (c) ECMWF and (d) RCA and RACMO are compared with the observed overlap calculated for the respective model mean time average (Table 1). The model cloud fractions (thin dashed–dotted line in (c) and dashed and dotted lines in (d)) and the radar volume and area fractions (grey bands) are also given.

maximum-random (MR, Eq. (5)), random (RAN, Eq. (6)) to minimum (MIN, Eq. (7)) according to the following recursive formulas:

$$A_{1,j}^{\mathrm{MAX}} = \max\left(a_j, A_{1,j-1}^{\mathrm{MAX}}\right), \tag{4}$$

$$A_{1,j}^{\mathrm{MR}} = 1 - \left(1 - A_{1,j-1}^{\mathrm{MR}}\right)\frac{1 - \max\left(a_j, a_{j-1}\right)}{1 - a_{j-1}}, \tag{5}$$

$$A_{1,j}^{\mathrm{RAN}} = 1 - \left(1 - a_j\right) * \left(1 - A_{1,j-1}^{\mathrm{RAN}}\right), \tag{6}$$

$$A_{1,j}^{\mathrm{MIN}} = \min\left(1, a_j + A_{1,j-1}^{\mathrm{MIN}}\right), \tag{7}$$

where $A_{1,j}$ is the accumulated cloud cover between level 1 (TOA) and level j, and a_j is the cloud area fraction at level j. To calculate the overlap from the surface (i.e., level N), the calculations were made in the reverse order. The observed mean cloud cover from the surface and TOA was 76% for September, in between the maximum overlap value of 69% and the random overlap value of 84%. MR overlap gave a cloud cover of 73%. The overlap assumptions deviate most from the observed overlap at the maximum in cloud cover at 2 km. This leads to a larger error calculating the overlap from the surface and upwards, as compared to the TOA and downwards, due to the accumulation of errors throughout the atmosphere.

Since the observed cloud cover was close to MR overlap, we investigated how the MR assumption could be altered to give larger cloud covers. We could derive an overlap parameter for the accumulated cloud cover similar to the two-layer parameters, but it would be for a mixture of continuous and non-continuous clouds and a function of height. Therefore, it would not be easy to interpret or to apply. The mean observed overlap diverges from maximum overlap towards random just before the position of the maxima in cloud cover, where the gradient in cloud cover was the largest (Fig. 9a and b). This result was also found for individual clouds. Therefore, we defined a simple version of maximum-random overlap (MR grad) for which continuous clouds are in maximum overlap, but if the absolute change in cloud fraction between two levels was more than a certain value, γ, they were randomly overlapped according to:

$$A_{1,j}^{\mathrm{MR\ grad}} = \begin{cases} 1 - \left(1 - A_{1,j-1}^{\mathrm{MR\ grad}}\right)\frac{1-\max\left(a_j, a_{j-1}\right)}{1-a_{j-1}} & |a_j - a_{j-1}| < \gamma \\ 1 - \left(1 - a_j\right)^{*}\left(1 - A_{1,j-1}^{\mathrm{MR\ grad}}\right) & |a_j - a_{j-1}| > \gamma \end{cases}. \tag{8}$$

In Fig. 9, γ=17%, which is equivalent to 47% km^{-1} for the 360 m vertical resolution radar data. MR grad overlap gave a cloud cover of 76% for September, which was closest to the observations (Fig. 9a and b).

Before we turn to the whole overlap matrix, we show examples of the overlap calculated for the models (Fig. 9c and d). The difference between the radar volume and area fractions is fairly small for the 60 vertical levels of the ECMWF model. Therefore, the overlap calculated from the ECMWF plane-parallel clouds can be compared to the radar

overlap calculated from the area fractions. Due to compensating errors in model vertical cloud fractions (i.e., all models overestimated high clouds and underestimated mid-level clouds), the mean value of the ECMWF cloud cover using MR overlap was fairly close to the observed value at the surface. For RACMO and RCA with only 24 vertical levels, the radar-derived volume and area fractions differ more from each other (Fig. 9d). However, since all model vertical cloud fractions were of similar magnitude, the RACMO and RCA cloud covers were, like for the ECMWF model, close to the radar observed cloud cover for the wrong reasons. The RCA model had less overestimation of high clouds but more clouds below 2 km which produced a surface cloud cover larger than for the other models. Since the high altitude model volume cloud fractions were even larger than the radar area fractions, the overestimate of model high clouds would be even larger if the model subgrid-scale horizontal variability was considered. This illustrates how different errors in model vertical cloud distributions might be concealed if only the ground or TOA model cloud covers are validated with observations.

To evaluate the overlap at all levels, we calculated the whole overlap matrix:

$$\begin{bmatrix} A_{N,1} & A_{N-1,1} & A_{N-2,1} & \cdot & \cdot & A_{3,1} & A_{2,1} & A_{1,1} \\ A_{N,2} & A_{N-1,2} & \cdot & & \cdot & A_{3,2} & A_{2,2} & \cdot \\ A_{N,3} & \cdot & & & \cdot & A_{3,3} & \cdot & \cdot \\ \cdot & & & & \cdots & & & \\ & & & \cdots & & & & \\ \cdot & \cdot & \cdot & \cdots & & & & \cdot \\ A_{N,N-2} & A_{N-1,N-2} & A_{N-3,N-3} & & & & \cdot & A_{1,N-2} \\ A_{N,N-1} & A_{N-1,N-1} & \cdot & & & \cdot & A_{2,N-1} & A_{1,N-1} \\ A_{N,N} & \cdot & \cdot & & \cdot & A_{3,N} & A_{2,N} & A_{1,N} \end{bmatrix} \tag{9}$$

for the different overlap assumptions. The individual matrix elements, $A_{i,j}$, represent the accumulated cloud fractions (i.e., cloud coverage) viewed from level to level j as observed and calculated using the overlap assumptions in Eqs. (4)–(8). The diagonal elements $A_{i,i}$ are equal to zero. As before, level 1 is at the TOA and level N is at the surface. The matrix is symmetric (unless the overlap formulation is dependent of the distance; see below) and only the upper, or lower, triangular part of it has to be calculated.

The observed mean cloud overlap matrix for September for radar grid boxes of 360 m and 60 min is shown in Fig. 10a. Both upper and lower triangular parts of the observed matrix are plotted so that the corresponding bias and root mean square errors for the different overlap assumptions (Fig. 10b–h) can be compared easily to the values of the overlap matrix elements. The overlap from TOA in Fig. 9a corresponds to the top row and last column of Fig. 10a, as the grey arrows indicate. The overlap from the surface (Fig. 9b) corresponds to the bottom row and first column of Fig. 10a, as indicated by the black arrows. Relative to the observed overlap matrix, maximum and MR overlap produced too small cloud covers at all levels, whereas random and minimum overlap yielded too large cloud covers. The MR gradient overlap had a small positive bias and a slightly larger RMSE than for MR overlap.

Another alternative to MR overlap would be to use the "exact" formulation. As pointed out by Li (2000), the recursive formula in Eq. (5) given by Geleyn and Hollingsworth

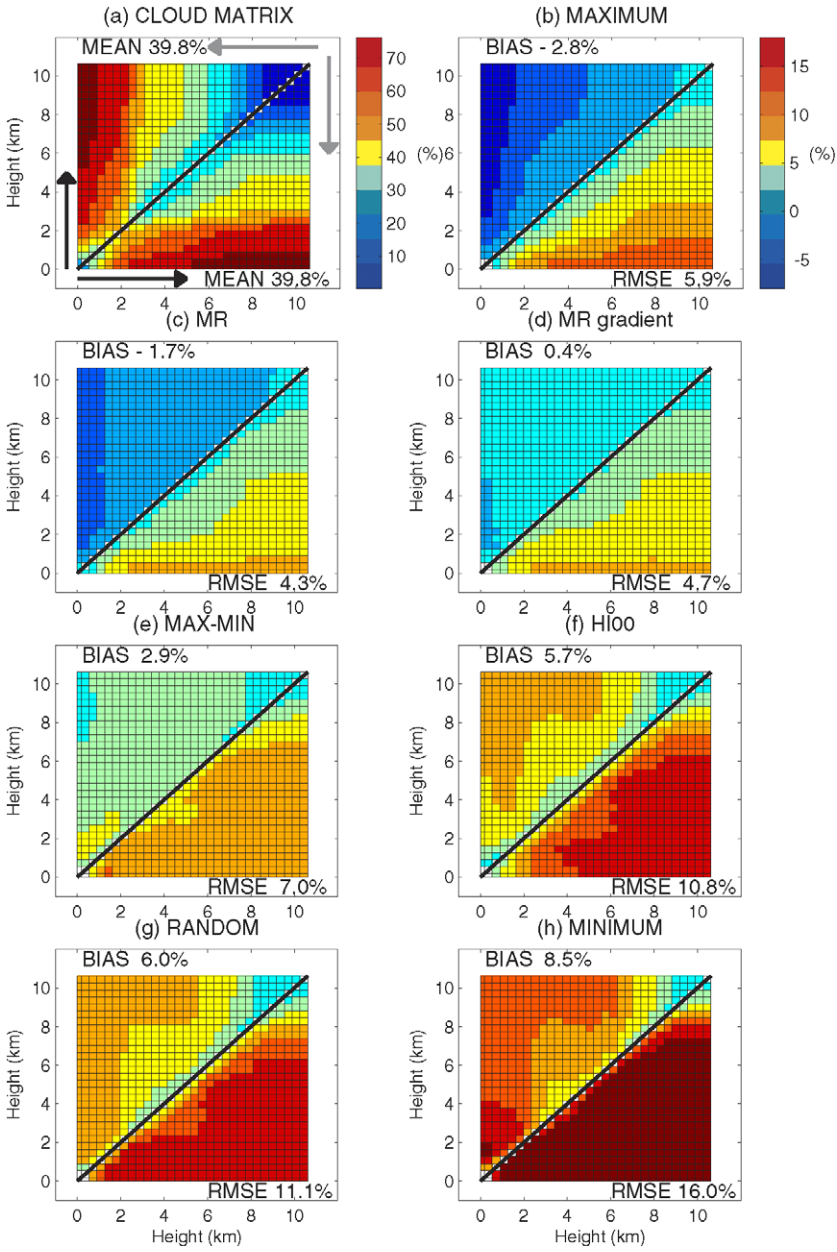

Fig. 10. (a) The cloud overlap matrix for September for 360 m vertical resolution and 60 min temporally averaged observations as a function of height. The arrows indicate the accumulation from above (grey) and from below (black). (b–h) The bias (above the diagonal) and RMSE (below the diagonal) for maximum to minimum overlap.

(1979) does not give exact MR overlap. One should instead first calculate maximum overlap for continuous cloud blocks and then apply random overlap for separate cloud blocks. However, we obtained only marginal changes for the cloud matrix with slightly smaller mean negative bias and larger RMSE (−1.5%, and 5.6%, respectively) compared to the recursive formula for MR overlap.

Finally, we tested the two-layer overlap parameters from Section 6 for calculating the accumulated cloud fractions in the overlap matrix. The errors in the overlap matrix using the parameterisation of HI00:

$$A_{i,j}^{\mathrm{HI00}} = \alpha^{*} A_{i,j}^{\mathrm{MAX}} + (1-\alpha)^{*} A_{i,j}^{\mathrm{RAN}} \quad \begin{cases} \alpha = \exp(-\Delta z/\Delta z_0) & \text{continuous clouds} \\ \alpha = 0 & \text{non-continous clouds,} \end{cases} \tag{10}$$

with Δz_0=1.6 km from Table 1 of HI00 for a 360 m and 60 min grid box and Δz as the vertical separation between layer heights, as illustrated in Fig. 10f. $A_{i,j}$ are the accumulated cloud fractions used in Eq. (9). Since the majority of clouds were thicker than 1.6 km for the averaged data (Fig. 8c), the cloud cover produced by this version of the HI00 parameterization was only slightly smaller than for random overlap (i.e., $\alpha \approx 0$ also for continuous clouds). The overlap matrix is not symmetric using Eq. (10) since it changes from maximum to random with the distance, and different values of cloud cover could be obtained if it is calculated from the surface or TOA. In Fig. 10f, it is shown as calculated from below. The HI00 overlap parameterization starting from TOA gave an error pattern close to the error for random overlap.

The errors using the maximum–minimum parameter, i.e.,

$$A_{i,j}^{\mathrm{Max-Min}} = \beta^{*} A_{i,j}^{\mathrm{MAX}} + (1-\beta)^{*} A_{i,j}^{\mathrm{MIN}} \tag{11}$$

with a fixed value of β=0.5, is illustrated in Fig. 10e. The choice for β is reasonable as the observations (Fig. 8) were fairly close to this value for all clouds. This approach gave a smaller cloud cover in the mean than the HI00 parameterization and therefore a smaller positive bias.

We calculated the overlap matrix for all the overlap assumptions for different vertical spatial and horizontal temporal resolutions from both radar data sets for the BBC period. The mean biases and RMSEs for the matrix are shown in Fig. 11. The mean error patterns are the same for both months, with maximum and maximum-random overlap producing too small cloud covers with a mean negative bias of 3–4%, whereas the two-layer parameterizations, random and minimum overlap, produce too large cloud covers by 5–12%. The MR gradient overlap has the smallest bias and an RMSE error comparable to the MR value. For longer time averages, the errors were larger for both radars, as could be expected since information on the exact position of a cloud element is gradually destroyed with averaging. Since the GKSS radar had higher frequency raw data (more pixels per time average) than the KNMI radar, it has a larger error for the same time average. For higher vertical resolution, any error in overlap will magnify, particularly for random and minimum overlap, since larger cloud covers are obtained. This accumulation of errors with

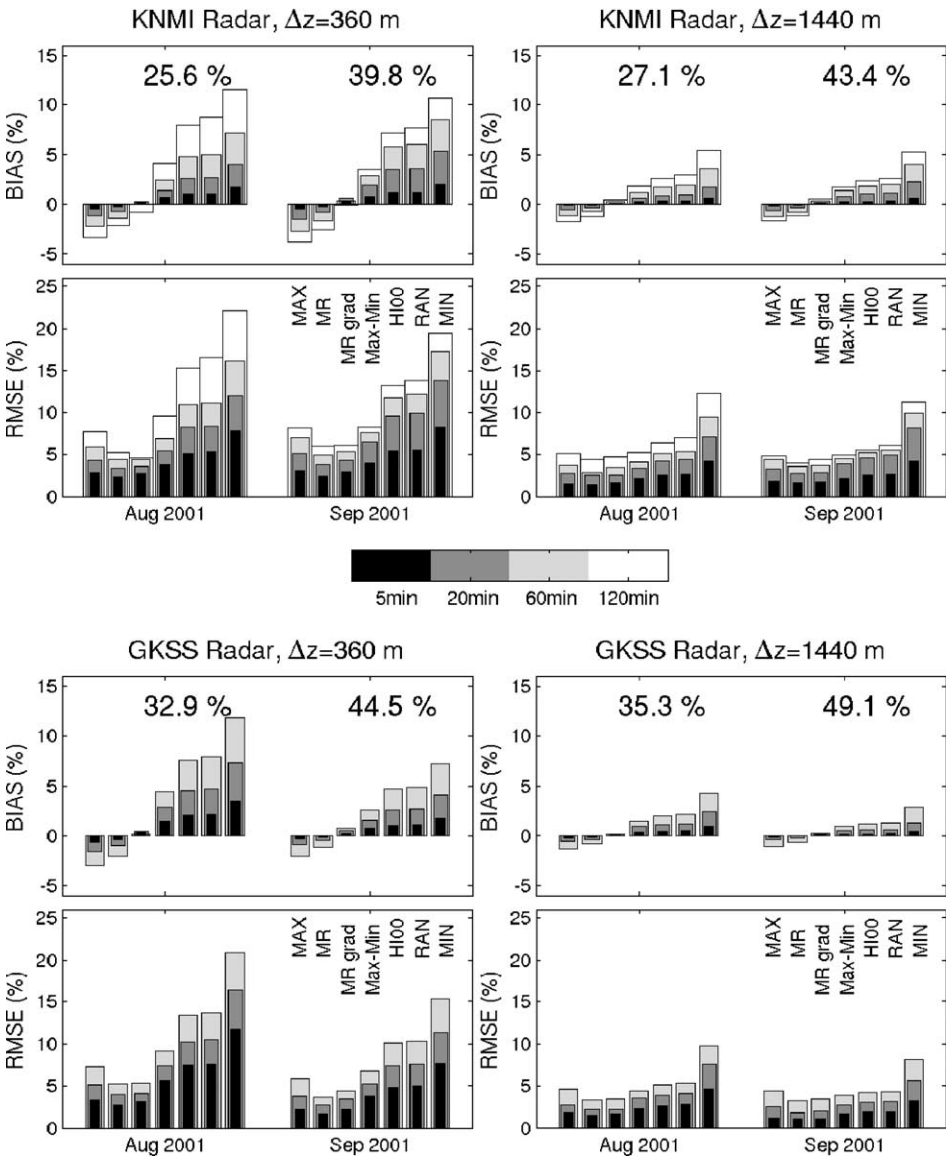

Fig. 11. Mean cloud matrix bias and RMSE for August and September for the KNMI and GKSS radars at different vertical resolutions of 360 m and 1440 m and different temporal averages from 5 min to 120 min. There was an upper limit of 90 min for the GKSS radar since it operated less than 12 h/day. All overlap assumptions are shown except "MR exact" since it produced results close to the MR values. The mean observed accumulated cloud covers for the matrix are given as numbers.

height (the number of levels) is also obvious in Figs. 9 and 10. The error patterns were similar when calculating the overlap matrix for unequally spaced vertical levels of the models (not shown).

The MR gradient bias was smallest when continuous clouds were in random overlap for γ larger than 15–20% for all the tested vertical spatial and temporal resolutions. The results in Fig. 11 are shown for γ=17%. A possible explanation as to why the maximum-random gradient overlap worked for both months and for different resolutions could be the result of a "variable" de-correlation length applicable for different thick clouds. Continuous clouds could be in maximum overlap in the interior, but near edges (i.e., top, bottom, or sides) where there is a larger change in cloud cover, they might be closer to random overlap independent of the separation distance as discussed in Section 6. The reason the results are different from the two-layer approach, for which the clouds were found to be mainly in random overlap at large separations, could be explained by again considering a slanted continuous cloud. Even if two individual clouds at a certain distance from each other are randomly placed, the overlap of one of the clouds with the accumulated cloud fractions of all levels in between would be larger than due to pure random overlap (i.e., a smaller cloud cover).

The gradient approach might be generally applicable for different cloud systems, since there are large gradients in cloud cover in cirrus anvil layers, and for shallow convection in the boundary layer, where protruding cloud parts can occur. But it might also work when unrelated small cloud elements are included within grid box averages, since they are more likely to be in random, or even minimum, overlap. We have repeated the analyses for four randomly chosen months during 2001 and 2003, other than the BBC period, and the results were similar (not shown). Moreover, the results showed surprisingly little dependence on the resolution or season. However, since the RMSE for the MR gradient approach was not much smaller than for MR overlap, there is room for improvement. Instead of using a fixed value for γ, deciding when continuous clouds are in random overlap, it could be made dependent on the model vertical and horizontal resolution and possibly on the cloud type by using, for example, the wind shear.

8. Summary and discussion

We have assessed the cloud vertical structure and cloud overlap of four large-scale models using two ground-based cloud profiling radars at Cabauw. Wind variations with height could potentially affect the radar-derived cloud fractions, giving rise to collocation errors in the time-average approach. Therefore, we used the maximum and minimum advective time scales in the grid columns to provide uncertainties in the point-to-space transformation of the radar observations. The model mean vertical cloud fraction distributions were in fairly good agreement with the radar measured fractions. However, the models overestimated high and low clouds and underestimated clouds at mid-levels, confirming results of previous studies that used one fixed advective time scale (Hogan et al., 2001). Despite different horizontal and vertical spatial resolutions, different cloud schemes, and different modes of operation, the model error structures were similar and to a large degree independent of the wind speed used to derive the radar cloud fractions.

The models underestimated the height of the lowest cloud base. This was also verified from measurements of cloud bases by six lidars in a network surrounding Cabauw. Clouds occurred more frequently in the models, but with less amounts when present. The models

overestimated the occurrences of small cloud fractions and underestimated the occurrences of clear-sky and overcast. This is contrary to findings by Hogan et al. (2001) who found similar partial cloudiness for the ECMWF model and radar observations. However, they modified the model cloud fractions to include snow, which is detected by the millimetre-wave radar but not normally included in the model cloud fractions. This approach did not improve the cloud fraction distribution for the ECMWF model in this study. For larger horizontal spatial scales, the observations were less "U-shaped," as expected, but even at 5 km spatial resolution, fractional cloudiness occurred, implying a potential need for cloud overlap parameterizations for high resolution models.

The large difference between modelled and observed high altitude cloud was similar for all models, which points to common model problems or insufficient radar sensitivity for detecting all types of high clouds. Our results support the previous findings by Hogan et al. (2001) that the ECMWF model overestimates high clouds above 7 km, even though our study used a more sensitive radar. Overestimation of high clouds by RACMO is also confirmed by satellite observations (Van Meijgaard et al., 2001), although these high model clouds might have optical thicknesses below satellite and radar thresholds of detection (Wyser and Jones, 2005). Even if model data are filtered to be comparable to the observations, only by removing or adding high clouds in the actual model radiation scheme could we reveal if they are radiatively significant for the model climate. Nonetheless, the errors could be due to the model cloud schemes or errors in the large-scale variables, since the cloud fractions for all the models are mainly determined by the relative humidity. To explore fully model shortcomings, we would need to look at longer time periods, and it would be informative to separate different cloud types. Studies in this direction have been done by Luo et al. (2003), who used cloud radar data to evaluate the properties of cirrus clouds in a CRM.

We found that observed clouds were thinner than the typical vertical resolution of the forecast and climate models, confirming the results of previous cloud-radar studies (Mace et al., 1997; Dong et al., 2000) and global studies using rawinsonde data (Wang et al., 2000). The radar-derived volume fractions were smaller than the radar-derived cloud area fractions. This type of deviation from the geometrical plane-parallel assumption made it difficult to evaluate the model overlap schemes, particularly for the regional climate models with coarser vertical resolution. The model (volume) fractions could be transformed into model area fractions using the information from the radar measurements and this could be taken into account in the large-scale radiation calculations. Future work will consider the impact of the combined subgrid-scale overlap with the standard overlap discussed below on the model radiative fluxes.

In this study, we did a preliminary comparison of radar and model cloud cover using the model volume cloud fractions. The combination of overestimates of model clouds at high levels and underestimates at mid-levels led to a cancellation of errors in the cloud cover at the surface and the TOA for all models. Since the model (volume) cloud fractions were larger than the radar area fractions at high levels, overestimation of cloud cover at high levels would also occur if model subgrid horizontal variability was considered. If the overestimate of clouds at high levels and underestimation at mid-levels are true features of large-scale models, standard approaches for validation of cloud cover with satellite and synop observations could be in error.

Previous studies of cloud-radar overlap have been performed by considering the overlap of two layers (HI00 and MB02). Our results agree with these studies in that non-continuous clouds were close to random overlap. The overlap for continuous clouds varied exponentially from maximum to random at certain de-correlation lengths depending on the vertical spatial and temporal averages of the data, similar to what HI00 found for Chilbolton, UK. We expressed a two-layer cloud overlap as a mixture of maximum and minimum overlap, thereby avoiding negative correlations. We also derived the radar cloud–overlap matrix to illustrate the overlap throughout the vertical extent of the atmosphere. The observed combined cloud cover across all layers was close to maximum-random overlap at all levels.

A new version of maximum-random overlap, which uses random overlap for continuous clouds when the vertical gradient in cloud fraction is sufficiently high, gave the smallest mean error for the cloud matrix for all spatial and temporal resolutions. By using the gradient in cloud fraction, we obtained a variable de-correlation length with a dependence on cloud thickness. This approach provides a simple way of taking into account the smaller degree of overlap for slanted clouds, anvils, and completely unrelated cloud elements that can be included within larger grid boxes. In this study, we presented results from only 2 months of the BBC period, but the results were robust as we obtained similar results for different seasons and cloud types (e.g., frontal, boundary layer, and convective clouds) at Cabauw. The gradient approach could be improved by making the overlap dependent on the vertical and horizontal spatial scale of the model, as well as the cloud type, and it should be tested at other locations.

Acknowledgements

The authors would like to thank Colin Jones (SMHI), Erik Van Meijgaard (KNMI), Adrian Tompkins (ECMWF), and Felix Ament (University of Bonn) for supplying the model output. Comments by Klaus Wyser (SMHI), Erik Van Meijgaard, and Colin Jones have helped to improve the manuscript. We are grateful to three anonymous reviewers for their helpful suggestions. This work was partly performed within the CLIWA-NET project sponsored by the EU under contract no. EVK2CT-1999-00007.

References

Barker, H.W., Stephens, G.L., Fu, Q., 1999. The sensitivity of domain-averaged solar fluxes to assumptions about cloud geometry. Q. J. Royal Meteorol. Soc. 125, 2127–2152.

Barker, H.W., Stephens, G.L., Partain, P.T., Bergman, J.W., Bonnel, B., Campana, K., Clothiaux, E.E., Clough, S., Cusack, S., Delamere, J., Edwards, J., Evans, K.F., Fouquart, Y., Freidenreich, S., Galin, V., Hou, Y., Kato, S., Li, J., Mlawer, E., Morcrette, J., O'Hirok, W., Räisänen, P., Ramaswamy, V., Ritter, B., Rozanov, E., Schlesinger, M., Shibata, K., Sporyshev, P., Sun, Z., Wendisch, M., Wood, N., Yang, F., 2003. Assessing 1D atmospheric solar radiative transfer models: interpretation and handling of unresolved clouds. J. Climate 16, 2676–2699.

Beesely, J.A., Bretherton, C.S., Jakob, C., Andreas, E.L., Intreri, J.M., Uttal, T.A., 2001. A comparison of cloud and boundary layer variables in the ECMWF forecast model with observations at the SHEBA ice camp. J. Geophys. Res. 105, 12337–12349.

Crewell, S., Simmer, C., Lohnert, U., Venema, V., Feijt, A., van Meijgaard, E., van Lammeren, A., Bloemink, H., Jolivet, D., Wendisch, M., Schmidt, S., Schroder, M., Willẽn, U., Quante, M., Meywerk, J., Krasnov, O., Trautmann, T., Garcia, S.G., Pfeilsticker, K., Scholl, T., 2004. The BALTEX Bridge Campaign: an integrated approach for a better understanding of clouds. Bull. Am. Meteorol. Soc. 85, 1565–1584.

Dong, X., Minnis, P., Ackerman, T.P., Clothiaux, E.E., Mace, G.G., Long, C.N., Liljegren, J.C., 2000. A 25-month database of stratus cloud properties generated from ground-based measurements at the Atmospheric Radiation Measurement Southern Great Plain site. J. Geophys. Res. 105, 4529–4537.

Döscher, R., Willén, U., Jones, C., Rutgersson, A., Meier, H.E.M., Hansson, U., Graham, L.P., 2002. The development of the regional coupled ocean-atmospheric model RACMO. Boreal Environ. Res., 183–192.

Geleyn, J.F., Hollingsworth, A., 1979. Economical analytical method for the computation of the interaction between scattering and line absorption of radiation. Beitr. Phys. Atmos. 52, 1–16.

Hogan, R.J., Illingworth, A.J., 2000. Deriving cloud overlap statistics from radar. Q. J. Royal Meteorol. Soc. 126, 2903–2909.

Hogan, R.J., Jakob, C., Illingworth, A.J., 2001. Comparison of ECMWF winter-season cloud fraction with radar-derived values. J. Appl. Meteorol. 40, 513–525.

Illingworth, A.J., and the CloudNET team, 2004. Comparison of observed cloud properties at three ground based sites with their representation in operational models: the EU CloudNET project. Proceedings of the 14th International Conference on Clouds and Precipitation, Bologna, Italy, vol. 2, pp. 1334–1336.

Jakob, C., Pincus, R., Hannay, C., Xu, K.-M., 2004. Use of cloud radar for model evaluation: a probabilistic approach. J. Geophys. Res. 109, D03202.

Li, J., 2000. Accounting for overlap of fractional cloud in infrared radiation. Q. J. Royal Meteorol. Soc. 126, 3325–3342.

Luo, Y., Krueger, S.K., Mace, G.G., 2003. Cirrus cloud properties from a cloud-resolving model simulation compared to cloud radar observations. J. Atmos. Sci. 60, 510–525.

Mace, G.G., Benson-Troth, S., 2002. Cloud-layer overlap characteristics derived from long-term cloud radar data. J. Climate 15, 2505–2515.

Mace, G.G., Ackerman, T.P., Clothiaux, E.E., Albrecht, B.A., 1997. A study of composite cirrus morphology using data from a 94-GHz radar and correlations with temperature and large-scale vertical motion. J. Geophys. Res. 102, 13581–13593.

Mace, G.G., Jakob, C., Moran, K.P., 1998. Validation of hydrometeor occurrence predicted by the ECMWF model using millimeter wave radar data. Geophys. Res. Lett. 25, 1645–1648.

Manabe, S., Strickler, R.F., 1964. Evaluation and optimizaton of sampling errors for the Monte Carlo independent column approximation. J. Atmos. Sci. 21, 361–385.

Quante, M., Lemke, H., Flentje, H., Francis, P., Pelon, J., 2000. Boundaries and internal structure of mixed phase clouds as deduced from ground-based 95-GHz radar and airborne lidar measurements. Phys. Chem. Earth, Part B Hydrol. Oceans Atmos 25, 889–895.

Räisänen, P., Barker, H.W., 2004. Evaluation and optimization of sampling errors for the Monte Carlo independent column approximation. Q. J. Royal Meteorol. Soc. 130, 2069–2085.

Randall, D., Khairoutdinov, M., Arakawa, A., Grabowski, W., 2003. Breaking the cloud parameterization deadlock. Bull. Am. Meteorol. Soc. 84, 1547–1564.

Tian, L., Curry, J.A., 1989. Cloud overlap statistics. J. Geophys. Res. 94, 9925–9935.

Tiedkte, M., 1993. Representations of clouds in large scale models. Mon. Weather Rev. 121, 3040–3061.

Van Meijgaard, E., Crewell, S., 2005. Comparison of model predicted liquid water path with ground-based measurements during CLIWA-NET. Atmos. Res. 75, 201–226.

Van Meijgaard, E., Andrae, U., Rockel, B., 2001. Comparison of model predicted cloud parameters and surface radiative fluxes with observations on the 100 km scale. Meteorol. Atmos. Phys. 77, 109–130.

Wang, J., Rossow, W.B., Zhang, Y., 2000. Cloud vertical structure and its variations from a 20-yr global rawinsonde dataset. J. Clim. 13, 3041–3056.

Weare, B.C., 2001. Effect of cloud overlap on radiative feedbacks. Clim. Dyn. 17, 143–150.

Wyser, K., Jones, C.G., 2005. Modeled and observed clouds during SHEBA. J. Geophys. Res.